Therapeutic Delivery of miR-29b Enhances Radiosensitivity in Cervical Cancer

Tingting Zhang,[1,2,3] Xiang Xue,[1,2,3] and Huixia Peng[1]

[1]Department of Gynecology, The Second Affiliated Hospital of Medical College of Xi'an Jiaotong University, Xi'an, China; [2]Oncology Research Lab, Key Laboratory of Environment and Genes Related to Diseases, Ministry of Education, Xi'an, China

Radioresistant cervical cancer is likely to give rise to local recurrence, distant metastatic relapse, and decreased survival rates. Recent studies revealed microRNA mediated regulation of tumor aggressiveness and metastasis; however, whether specific microRNAs regulate tumor radioresistance and can be exploited as radiosensitizing agents remains unclear. Here, we find that miR-29b could promote radiosensitivity in radioresistant subpopulations of cervical cancer cells. Notably, therapeutic delivery of miR-29b mimics via R11-SSPEI nanoparticle, whose specificity has been proved by our previous studies, can sensitize the tumor to radiation in a xenograft model. Mechanistically, we reveal a novel function of miR-29b in regulating intracellular reactive oxygen species signaling and explore a potential application for its use in combination with therapies known to increase oxidative stress such as radiation. Moreover, miR-29b inhibits DNA damage repair by targeting phosphate and tension homology deleted on chromsome ten (PTEN), and overexpression of PTEN could partially rescue miR-29b-mediated homologous recombination (HR)-DNA damage repair and increase radiosensitivity. These findings identify miR-29b as a radiosensitizing microRNA and reveal a new therapeutic strategy for radioresistant tumors.

INTRODUCTION

Radioresistance is one of the primary factors that limit the effectiveness of current therapies for cervical cancer. Strategies for overcoming this resistance should readily translate into improved outcomes.[1–3] Combining chemotherapy with radiation improves outcomes but often increases toxicity. To overcome this problem, it is necessary to develop new strategies for overcoming this resistance.

A growing number of studies have demonstrated that therapeutic delivery of synthetic microRNAs could mimic endogenous tumor suppressor microRNAs and are a promising approach for treating cancer.[4–6] microRNAs are small, noncoding RNAs of ~22 nt in length that target multiple cellular processes and act as negative regulators of gene expression. There is mounting evidence suggesting that microRNAs such as let-7, miR-181a, and others are involved in radioresistance of tumors.[7–10] However, the role of microRNAs on cervical cancer radiotherapy is poorly understood. Therefore, the goal of this work is to assess the potential applicability of microRNA delivery, in combination with radiation therapy, to treat cervical cancer.

Our focus has been on miR-29b, which suppresses proliferation, migration, and invasion in several cancer cells.[11–14] It has been reported that miR-29b could be a key regulator of the phosphate and tension homology deleted on chromsome ten (PTEN)-serine-threonine protein kinase (AKT) pathway, which contributes to tumorigenesis and tumor metastasis.[15,16] In addition, it is becoming increasingly clear that PTEN has novel nuclear functions, including transcriptional regulation of the RAD51 gene, whose product is essential for homologous recombination (HR) repair of DNA breaks.[17,18] Restoration of miR-29b expression inhibits cell growth and invasion in several types of tumors.[19] Nonetheless, the potential benefit of systemically delivered miR-29b in combination with radiation remains unclear.

It is well-known that radiation-induced cell death is related to reactive oxygen species (ROS). We postulated that miR-29b could potentiate the therapeutic effects of radiation through generation of ROS signals. In this study, we show that miR-29b is downregulated in radioresistant subpopulations of cervical cancer cells derived from ionizing radiation (IR). We further show that miR-29b overexpression increased cellular radiosensitivity by directly regulating and inhibiting DNA double-strand break (DSB) repair and decreasing PTEN/phosphatidylinositol 3-kinase (PI3K)-AKT activity. We also demonstrated the therapeutic potential of systemic delivery of miR-29b, using cancer-specific poly-arginine-disulfide-linked polyetherimide (PEI) nanocarrier-encapsulated miR-29b mimic (R11-SSPEI/miR-29b), to enhance radiosensitivity in cervical cancer by using a xenograft mouse model of cancer. miR-29b inhibits DNA damage repair, increases the levels of ROS, and radiosensitizes tumor cells by targeting PTEN. Collectively, these results suggest that miR-29b delivery combined with radiation therapy may represent a new therapeutic approach for cervical cancer.

RESULTS

miR-29b Promotes Radiosensitivity and Is Downregulated in Radioresistant Tumor Cells

To identify the radiosensitivity effect of miR-29b in cervical cancer, we first assessed the expression level of miR-29b in cervical cancer cells.
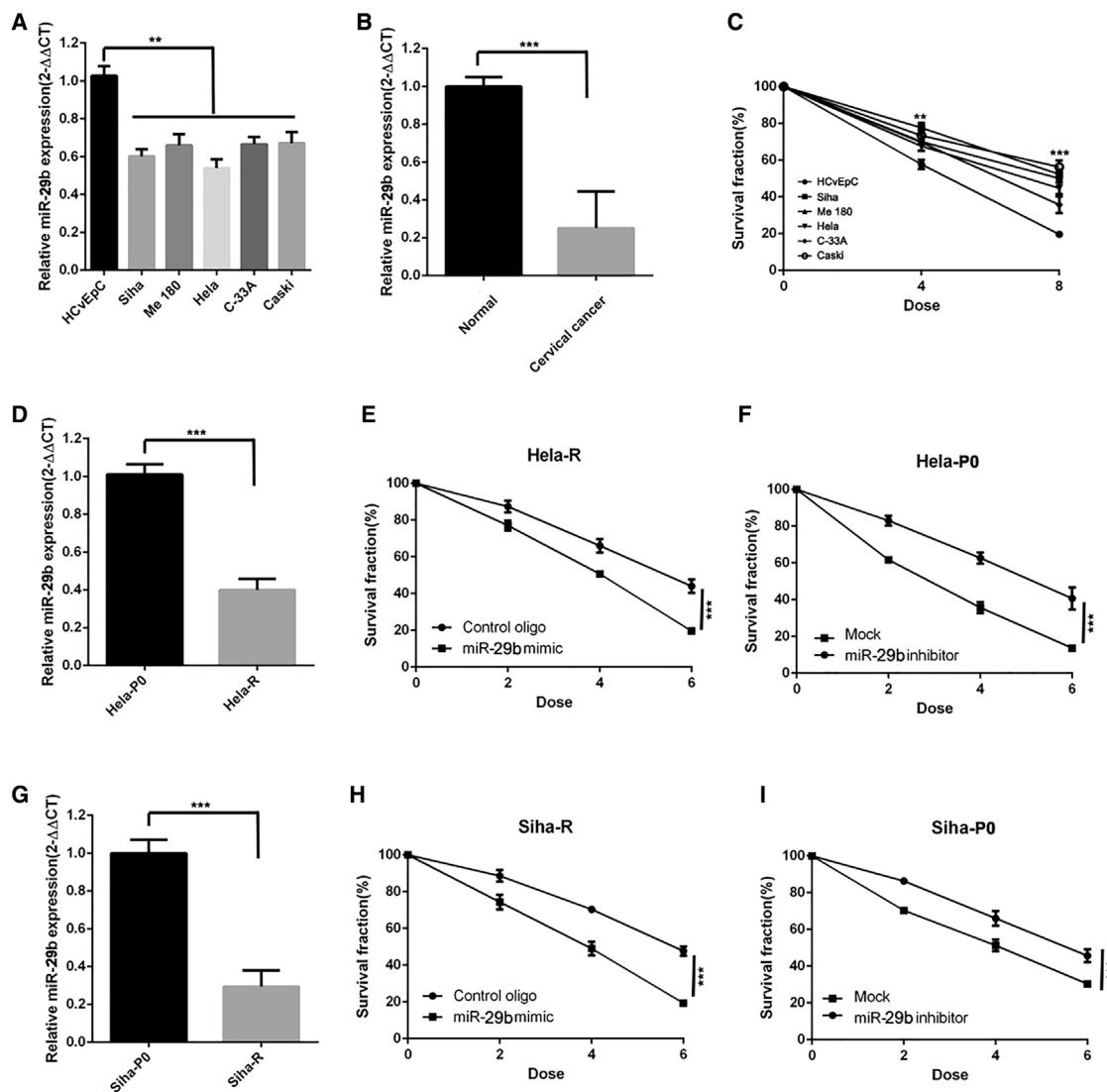
Figure 1. miR-29b Increases Radiosensitivity and Is Downregulated in Radioresistant Cervical Cancer Cells

(A) qPCR of miR-29b of normal cervical cell line (HCvEpc) and cervical cancer cell lines (Siha, Me 180, HeLa, C-33A, Caski). n = 3 samples per group. (B) qPCR of miR-29b of normal cervical tissue and cervical cancer tissues. n = 8 samples per group. (C) Clonogenic survival assays of normal cervical cell line and cervical cancer cell lines. n = 3 samples per group. (D) qPCR of miR-29b of HeLa-R cells relative to HeLa-P0 cells. n = 3 samples per group. (E) Clonogenic survival assays of HeLa-R cells transduced with miR-29. n = 3 wells per group. (F) Clonogenic survival assays of HeLa-P0 cells transfected with the miR-29 inhibitor. n = 3 wells per group. (G) qPCR of miR-29b of Siha-R cells relative to Siha-P0 cells. n = 3 samples per group. (H) Clonogenic survival assays of Siha-R cells transduced with miR-29. n = 3 wells per group. (I) Clonogenic survival assays of Siha-P0 cells transfected with the miR-29 inhibitor. n = 3 wells per group. Data are the mean of biological replicates from a representative experiment, and error bars indicate SEM. Statistical significance was determined by a two-tailed, unpaired Student's t test. The experiments were repeated three times. **p < 0.035; ***p < 0.01.

As shown in Figure 1, cervical cancer exhibited much lower levels of miR-29b in both cell lines and tumor tissues (Figures 1A and 1B), but higher clonogenic survival ability after irradiation (Figure 1C).

Moreover, to clarify how miR-29b affects radiosensitivity in cervical cancer, we established a radioresistant model. As shown in Figure S1, we used γ-IR to select the radioresistant subpopulation (designated as HeLa/Siha-R cells) from the parental HeLa/Siha-P0 human cervical cancer cell line. In this model, miR-29b was dramatically downregulated in HeLa-R cells compared with the parental HeLa-P0 cells (Figure 1D). Next, we performed gain-of-function and loss-of-function assays of miR-29b in cervical cancer cells. As shown in Figure 1E, transfection of HeLa-R cells with miR-29b mimic could sensitize these cells to radiation. Conversely, downexpression of miR-29b in HeLa-P0 cells conferred radioresistance on these cells (Figure 1F). Similar effects were also observed in Siha cervical cancer cells (Figures
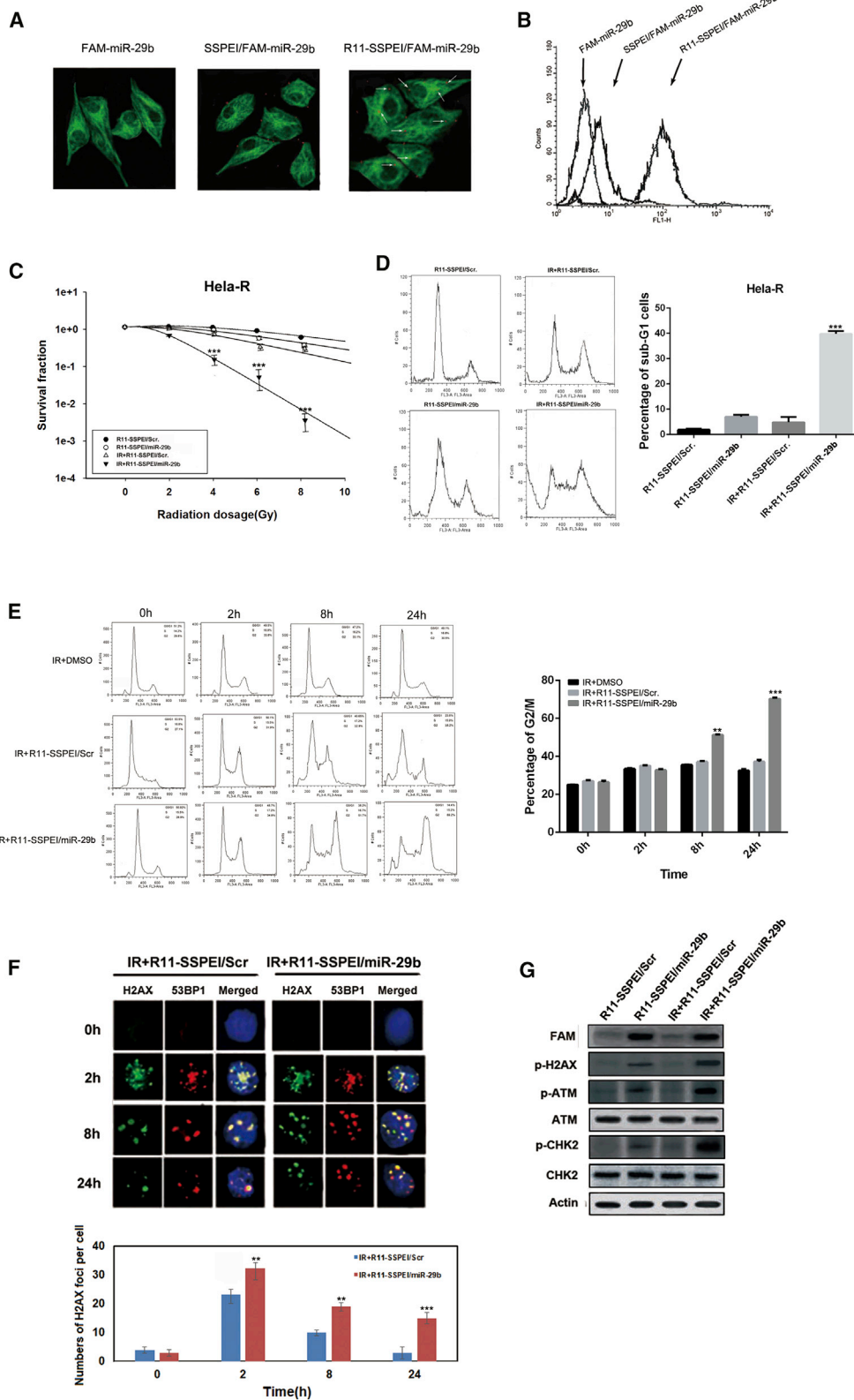
1G–1I). Thus, the observed effect of miR-29b is not limited to the HeLa cell line.

Intracellular Delivery of miR-29b Enhances Radiosensitivity in Radioresistant Cervical Cancer Cells and Is Associated with Compromised DSB Repair

Our previous data had already shown that R11-SSPEI could deliver microRNA to prostate cancer cells. In this study, we first verify whether the R11-SSPEI-mediated miR-29b has the same intracellular uptake pattern in cervical cancer as our previous study in prostate cancer. As shown in Figure 2A, FAM-labeled miR-29b encapsulated with R11-SSPEI was added to cells. Confocal microscope images displayed that the fluorescence spot of FAM-miR-29b was detected at 1 h in the cytoplasmic area, indicating efficient delivery of miR-29b mediated by R11-SSPEI, inside the cervical cancer cells. Confocal microscopy images show that internalization of FAM-labeled miR-29b was found in the cytoplasmic area of HeLa-R cells at 1 h (arrow, red spot). The cytoplasmic regions of HeLa-R cells were stained with the CM-DiI fluorescence tracker (green). Next, to more precisely elucidate the cellular internalization of the targeting nanovectors, we used flow cytometry to quantify the cell uptake efficiency (Figure 2B). The percentages of the HeLa-R cells treated with FAM-miR-29b, SSPEI/FAM-miR-29b, and R11-SSPEI/FAM-miR-29b were 6.1%, 5.3%, and 88.9%, respectively. We also evaluated the uptake efficiency of the nanoparticles in Siha cells by confocal image and flow cytometric analysis (data not shown). The above results indicate that R11-SSPEI nanocarrier could enhance the intracellular uptake in cervical cancer cells.

We then assessed whether R11-SSPEI/miR-29b increases the radiosensitivity of HeLa-R to IR. The viability of cells was determined using clonogenic assay after different treatments. We found that HeLa-R cells were more susceptible to combined treatment than IR alone (Figure 2C), and R11-SSPEI/miR-29b significantly enhanced the effects of IR on HeLa-R cells, but not R11-SSPEI/Scr.

We further investigated whether R11-SSPEI/miR-29b induces cell death in HeLa-R cells. After treatment with different nanoparticles or IR+nanoparticle combination, cells were incubated for 48 h, and cell-cycle analysis was performed by flow cytometry. As shown in Figure 2D, the proportion of sub-G1 cells treated with nanoparticle alone was similar to that in the control nanoparticle group, and IR treatment did not increase the proportion of sub-G1 cells in HeLa-R cells. However, a combination of R11-SSPEI/miR26b and IR synergistically increased the sub-G1 population in HeLa-R cells after 48 h. These results indicate that R11-SSPEI/miR-29b can effectively increase IR-induced apoptosis in HeLa-R cells.

In addition, to evaluate the effect of miR-29b on cell-cycle arrest in radioresistant HeLa-R cells, we treated cells with different treatments combined with IR. Cells were then harvested at various time points and subjected to cell-cycle analysis. Our data showed that when treated with IR, as well as IR+R11-SSPEI/Scr, the number of HeLa-R cells arrested in G2/M phase gradually increased from 0 to 24 h (Figure 2E). In contrast, a combination treatment with R11-SSPEI/miR26b and IR led to a synergistic G2/M cell-cycle arrest observed at 24 h. These results suggest that miR-29b-induced cell death in radioresistant HeLa-R cells may be mediated through G2/M cell-cycle arrest.

It is well-known that the recruitment of phospho-γ-H2AX and 53BP1 at the damage sites often indicates an early step in response to DSB. We therefore examined the effect of miR-29b on radiation-induced DNA DSBs and the kinetics of DNA repair. HeLa-R cells were treated with R11-SSPEI/Scr or R11-SSPEI/miR-29b (10 nM) for varying amounts of time and subjected to immunofluorescence staining for phospho-γ-H2AX (green) and 53BP1 (red) foci. As shown in Figure 2F, the co-localization of γ-H2AX and 53BP1 foci significantly increased in HeLa-R cells upon exposure to IR+R11-SSPEI/miR-29b for 2 h compared with the IR+R11-SSPEI/Scr group. However, the remaining foci were almost abolished in HeLa-R cells treated with IR at 24 h. Nevertheless, in cells treated with IR+R11-SSPEI/miR-29b, the high level of foci formation remained observable in HeLa-R cells at 24 h, and we repeat it in Siha cells (Figure S2). In agreement with our previous results, IR+R11-SSPEI/miR-29b increased foci formation in Siha cell lines compared with cells stably transfected with a control vector at 8 and 24 h, but there was not a significant difference at 2 h. We subsequently profiled the status of the key molecules associated with DNA DSB, and the results indicate that the expression of phosphorylated γ-H2AX, CHK2, and ATM increased in cells treated with a combination of R11-SSPEI/miR-29b with IR compared with control (Figure 2G). These results indicate that R11-SSPEI/miR-29b enhances IR-induced DSB in HeLa-R cells.

Figure 2. Intracellular Delivery of miR-29b Enhances Radiosensitivity in Radioresistant Cervical Cancer Cells and Is Associated with Compromised DSB Repair

(A) Confocal microscopy images show the internalization of FAM-labeled miR-29b (arrow, red spot) and the cytoplasmic regions stained with the CM-DiI fluorescence tracker (green). (B) FACS analysis showing the uptake of fluoresceinated miR-29b, SSPEI, and R11-SSPEI after 1-h incubation of HeLa-R cells. (C) Clonogenic survival assays of HeLa-R cells treated with IR (0–10 Gy) alone, or R11-SSPEI/Scr (10 nM), R11-SSPEI/miR-29b combined with IR. (D) Flow cytometry of HeLa-R cells treated with R11-SSPEI/Scr, R11-SSPEI/miR-29b (10 nM) alone, IR (2 Gy) alone, and a combination of nanoparticle and IR. The percentages of cells in sub-G1 were calculated and plotted as intensity bars (right panel). (E) Flow cytometry of HeLa-R cells exposed to R11-SSPEI/Scr, R11-SSPEI/miR-29b (10 nM) alone, IR (2 Gy) alone, or nanoparticle for 1 h prior to IR treatment. The percentage of cells in G2/M was calculated and plotted as intensity bars (right panel). (F) Confocal images of HeLa-R cells treated with a combination of R11-SSPEI/Scr, R11-SSPEI/miR-29b (10 nM) and IR (2 Gy) for the indicated time and immunostained for phospho-γ-H2AX (green) and 53BP1 (red) foci. (G) The expression levels of phosphorylated proteins (γ-H2AX, ATM, and CHK2) in cells treated with R11-SSPEI/Scr, R11-SSPEI/miR-29b, irradiation (IR), and nanoparticle combined with radiation for 24 h are shown. Actin expression is used as the loading control. The asterisk (*) indicates statistical significance ($p < 0.05$) determined by Student's t test. **$p < 0.035$; ***$p < 0.01$.

miR-29b Overexpression Augments Intracellular ROS Levels and Activated p38 Mitogen-Activated Protein Kinase Signaling Pathway

After finding that miR-29b overexpression may enhance radiation-induced DSBs, we next tested the effect of miR-29b on the oxidative stress response by analyzing intracellular ROS levels. ROS generation was significantly increased in Siha-R/HeLa-R with miR-29b overexpression, whereas ROS generation with stable integration of scramble sequence showed no obvious change 24 h after 2 Gy X-ray irradiation, as shown in Figure 3A. Moreover, miR-29b overexpression increased ROS levels in Siha-R/HeLa-R, which was abrogated in the presence of N-acetylcysteine (NAC; a ROS scavenger) (Figure 3B).

It was reported that ROS-mediated activation of p38 mitogen-activated protein kinase (MAPK) plays a pivotal role in the cell apoptosis.[20,21] Thus, to identify the signaling pathways involved in miR-29b overexpression-mediated radiosensitivity in cervical cancer, we determined whether p38 MAPK signaling pathway was activated. As shown in Figure 3C, miR-29b overexpression increased phosphorylated p38 and ATF2.

Taken together, these results indicated that miR-29b overexpression augments intracellular ROS levels and activated the p38 MAPK signaling pathway in cervical cancer.

miR-29b Regulates DNA Damage Repair and Radiosensitivity through PTEN

Recent studies established that miR-29b affected cancer proliferation, migration, and invasion through regulation of their direct target PTEN.[15,16] We attempted to understand whether miR-29b enhances radiosensitivity through PTEN. Increasing the endogenous miR-29b levels by either oligonucleotide transfection (*p < 0.05; Figures S3A and S3B) or nanocarrier transduction (Figures 4A and 4B) could significantly decrease PTEN expression both at the RNA and protein levels, and decreasing the miR-29b levels had the opposite effect. Moreover, to verify whether PTEN is a direct target of miR-29b, we cloned PTEN 3′ UTR, the sequence that contains the miR-29b binding sites, into the downstream luciferase open reading frame (Figure S3C). The co-transfection of miR-29b mimics and the PTEN-3′ UTR-wild vector into HeLa-R cells (pLuc-PTEN-3′ UTR) significantly decreased the luciferase activity compared with miR-NC mimics (Figure S3D). In contrast, the transfection of miR-29b inhibitors into HeLa-R increased the luciferase activity. However, the transfection of mimics or inhibitors of miR-29b with the mutant 3′ UTR vector (pLuc-PTEN-mut 3′ UTR) did not affect the luciferase activity.

Then we tested radiosensitivity in terms of clonogenic survival. HeLa-R cells with stable PTEN knockdown were more sensitive to the cytotoxic effects of radiation than were controls (Figure 4C). The same effect was observed by the overexpression of miR-29b (Figure 4D).

Next, we re-expressed PTEN, singly or in combination, in miR-29b downexpression HeLa-R cells. PTEN alone partially increased radio-

sensitivity and inhibited HR repair, and overexpression of PTEN led to a significant rescue (Figure 4E). Collectively, these results suggest that miR-29b inhibits HR-mediated DNA damage repair and increases radiosensitivity by targeting PTEN.

Because PTEN is an important negative regulator of PI3K-AKT signaling that is involved in the complex process of cancer apoptosis and progression, we examined whether miR-29b-PTEN axis inhibited HR-mediated DNA damage repair through regulating the PI3K-AKT pathway. As shown in Figure 4A, decreased PTEN levels could increase p-AKT expression. We then investigated whether a PI3K/Akt inhibitor sensitizes HeLa-R and miR-29b high-expressing cell to IR (Figure S4). We found that overexpression of PTEN led to decreased apoptosis after exposure to IR when compared with non-treatment controls, and treatment with the PI3K inhibitor, LY294002, had a mild effect. Furthermore, we re-expressed PTEN, singly or in combination with LY294002, in miR-29b-overexpressing HeLa-R cells (Figure S5). PTEN alone partially inhibits HR repair, LY294002 alone led to no significant effect, and PTEN in combination with LY294002 had no inhibition compared with PTEN treatment alone. Together, our results suggest that miR-29b could regulate PTEN-PI3K-AKT-mediated radiosensitivity in HeLa-R cells, but activation of the AKT pathway is not associated with HR-mediated DNA damage repair.

Therapeutic Delivery of miR-29b Enhances Radiosensitivity in Cervical Cancer

To examine the effect of miR-29b on radiosensitivity in vivo, we administered the nanoparticle R11-SSPEI/miR-29b in combination with fractionated irradiation to xenografted tumors in mice. Intramuscular (i.m.) tumors were created by inoculating 0.5×10^5 HeLa-R cells into the right leg of each mouse. When the tumors reached 5 mm in diameter, the mice were randomly assigned to one of six groups: vehicle, R11-SSPEI/miR-29b (/R11-SSPEI/Scr) only, radiation, and R11-SSPEI/miR-29b (/R11-SSPEI/Scr) plus radiation. The formulation was given as subcutaneous peritoneal injections at a dose of 5 mg/kg, and local irradiation was given to a total dose of 20 Gy, in 4-Gy fractions over 7 days. For the combination therapy condition, the nanoparticle was given 2 h before the radiation. We first investigated the accumulation of miR-29b mimics in the tumor and other tissues after intraperitoneal injection. At 12 h after the third dose of the microRNA, three mice per group were euthanized, and tissues were harvested for evaluation of miR-29b levels. Increased miR-29b levels were detected in the groups given R11-SSPEI/Scr (/R11-SSPEI/miR26b) or nanoparticle plus radiation in tumor (Figure 5A). Next, we analyzed the effect of the nanoparticle formulation on radioresponse of implanted HeLa-R cells as measured by tumor growth delay. For those experiments, the mice were killed when tumors reach 22–24 mm in diameter. Our in vivo results validated our previous in vitro observations in that R11-SSPEI/miR-29b significantly (p = 0.0026) sensitized cervical cancer cells to radiation (Figure 5B). The combination of R11-SSPEI/miR-29b and radiation delayed tumor growth to a mean (± SE) of 43.6 ± 2.2 days compared with the control (23.5 ± 1.1 days),
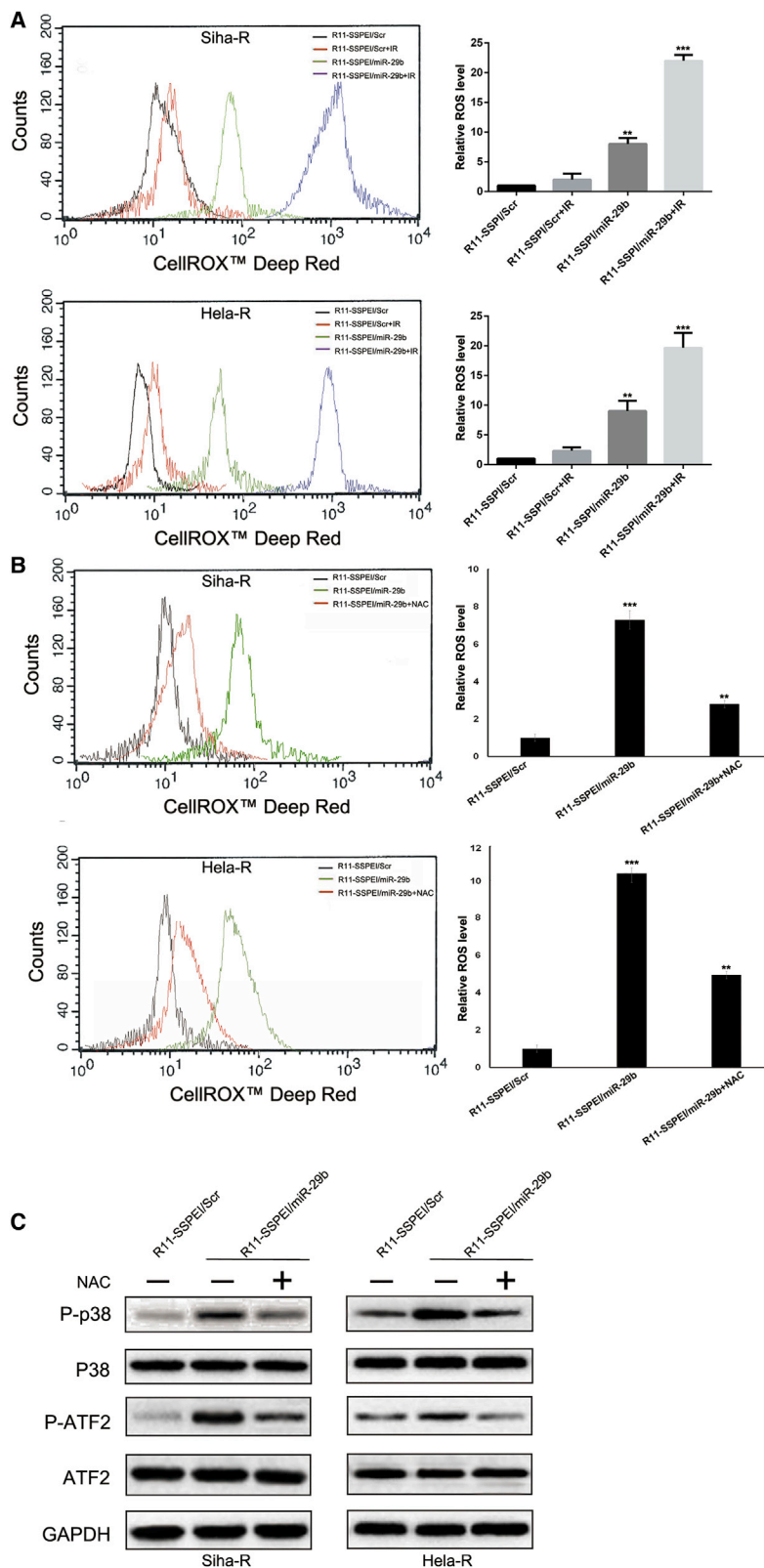
(A) R11-SSPEI/miR-29b-treated HeLa-R/Siha-R cells were assessed by flow cytometry for ROS generation by measuring the CELLROX Deep Red intensity, and the data were represented by histogram overlay (left panel). Line diagram representation of the dose-dependent ROS production in HeLa-R/Siha-R cells on treatment with different treatments (right panel). (B) Flow cytometric analysis of the miR-29b-induced ROS production with or without NAC, a pharmacological inhibitor of ROS, was determined and represented by histogram. (C) Detection of protein expression of p38 MAPK signaling pathway markers by western blot. The asterisk (*) indicates statistical significance (p < 0.05) determined by Student's t test. **p < 0.035; ***p < 0.01.
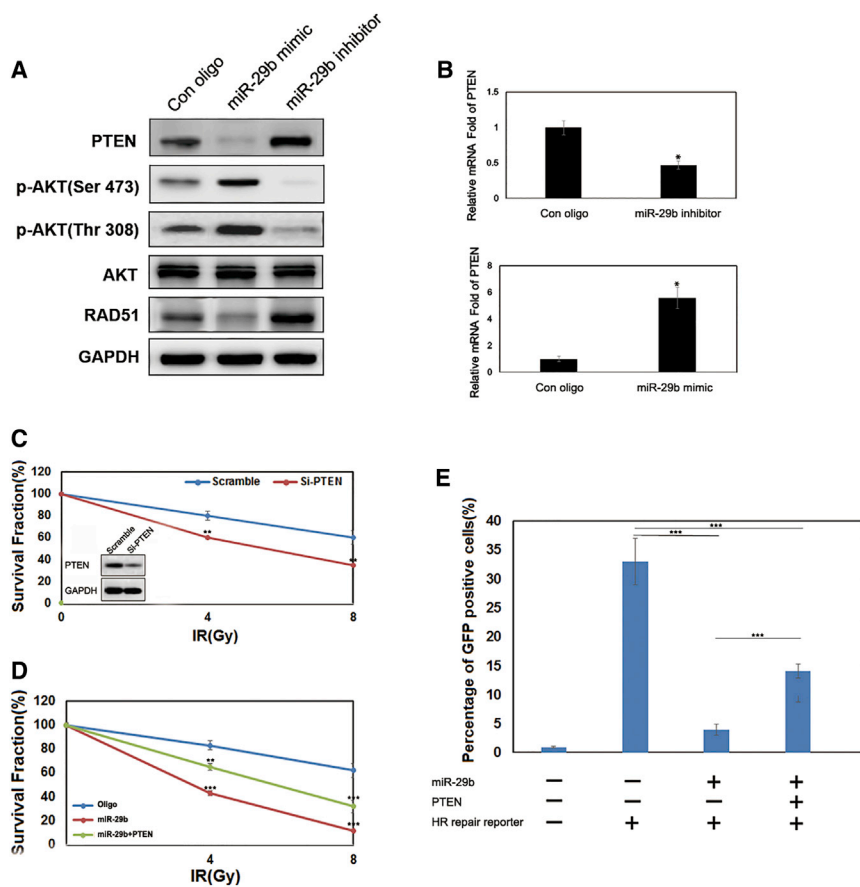
Figure 4. miR-29b Regulates DNA Damage Repair and Radiosensitivity through PTEN

(A) Immunoblotting of p-AKT, AKT, PTEN, and RAD51 in HeLa-R cells transfected with miR-29b mimics or the miR-29b inhibitor. (B) The mRNA expression levels of PTEN after the inhibition of miR-29b (top) or the over-expression of the same microRNA (bottom) in HeLa-R cells was detected using real-time qPCR. (C) Top: clonogenic survival assays of HeLa-R cells with or without ectopic expression of PTEN. Bottom: immunoblotting of PTEN and GAPDH. n = 3 wells per group. (D) Clonogenic survival assays of miR-29b-transduced HeLa-R cells with or without ectopic expression of PTEN. (E) HR repair assays of HeLa-R-GFP cells transfected with miR-29b alone or in combination with PTEN. n = 3 wells per group. Data are the mean of biological replicates from a representative experiment, and error bars indicate SEM. Statistical significance was determined by a two-tailed, unpaired Student's t test. The experiments were repeated three times. $*p < 0.05$; $**p < 0.035$; $***p < 0.01$.

above-mentioned clinical evidence, a targeted therapeutic strategy for miR-29b could potentially be developed.

In this study, we tested a novel approach to rendering treatment-resistant cervical cancer sensitive to therapy again. The key findings are as follows. First, both transient and nanoparticle transfection of cervical cancer cell lines (HeLa-R and Siha-R) with miR-29b constructs radiosensitized those cell lines (Figures 1 and 2). In addition, transfection of nanocarrier particle R11-SSPEI/miR-29b led to tumor growth delay in vivo (Figure 5). These findings strongly support the use of nanocarrier particle R11-SSPEI as a potential cancer therapeutic agent and agree with our previous studies in prostate cancers that R11-SSPEI nanocarrier could deliver microRNA to cancer cells and regulate biological functions.[30] Although miR-29b attenuates tumorigenicity and maintains stem characteristics in several human cancers,[31] this is the first study reporting miR29b as a radiosensitizer in cervical cancer.

R11-SSPEI/miR-29b-only (25.3 ± 2.5 days), or radiation-only (29.2 ± 1.5 days) groups. The normalized tumor growth delay was 18.3 ± 0.3 days, and the enhancement factor was 3.2 (Table 1).

DISCUSSION

Resistance to radiotherapy is a major obstacle in cervical cancer treatment. To improve the outcomes in these cases, identifying the mechanisms for cellular radioresistance is currently a heavily researched topic. Although numerous microRNAs are known to regulate the response to radiation, few of them can be targeted therapeutically. The importance of microRNAs as negative gene regulators for cancer is underscored by their functions in regulating multiple cellular processes, including the response to radiation. Consequently, they have the potential to be used as potential prognostic indicators.

miR-29 is a tumor suppressor and therefore affects cancer progression by regulating cell proliferation, survival, and metastasis.[22] Overexpression of miR-29b inhibits tumorigenesis[19,23,24] and angiogenesis.[25] Furthermore, miR-29b could reverse drug resistance in colorectal cancer[26] and ovarian cancer.[27] In addition, tissue expression levels and circulating levels of miR-29b have been shown to be associated with potential biomarkers for diagnosis and prognosis of colorectal cancer[28] and osteosarcoma patients.[29] On the basis of the
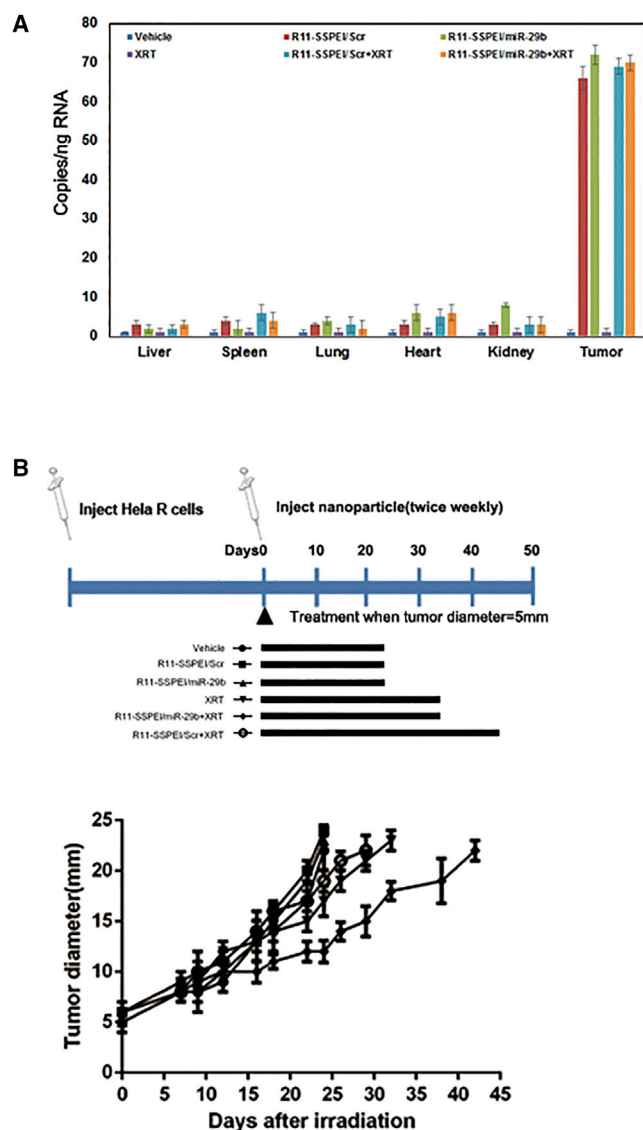
Next, because radiation-induced cytotoxicity is mediated primarily by the generation of ROS and ROS-driven oxidative stress, we investigated the effect of miR-29b on the oxidative stress response and found that overexpression of miR-29b led to higher ROS levels, and radical scavenger NAC could partially rescue this phenomenon (Figures 3A and 3B). In line with our findings, Xu et al.[32] demonstrated that miR-29b specifically regulates the self-renewal of mouse embryonic stem cells in response to ROS, generated by antioxidant-free culture, and overexpression of miR-29b could enhance ROS production and JNK phosphorylation to promote apoptosis in colorectal cancer.[26] Our findings complement these previous reports by demonstrating that miR-29b could promote radiation-induced cytotoxicity through increasing intracellular ROS levels.

A

B

Figure 5. Therapeutic Delivery of miR-29b Enhances Radiosensitivity in Cervical Cancer

(A) Systemic delivery of nanoparticle (R11-SSPEI/miR-29b or R11-SSPEI/Scr) leads to accumulation of miR-29b mimics in tumor after subcutaneous injection in mice. Two mice per treatment group were sacrificed 2 h after injections, and the tissues and transplanted tumors were harvested for total RNA extraction and evaluation of miR-29b levels. (B) Therapeutic delivery of miR-29b significantly sensitized lung cancer cells to radiation (XRT). The effect of R11-SSPEI/miR-29b on radioresponse of HeLa-R cells was measured by a tumor growth delay assay.

It is well documented that ROS regulates the expression of the p38/MAPK signaling pathway.[33] Once activated, p38 phosphorylates a variety of substrates in the cytoplasm and nucleus to regulate gene expression, cell cycle, drug resistance, and cell differentiation.[34] Our results showed that miR-29b overexpression increased phosphorylated p38 and ATF2, and these effects were partially reversed by a free radical scavenger NAC resulting in radiosensitivity (Figure 3C).

In accordance with our finding, Liu et al.[35] reported that increased miR-29b expression could suppress the activating p38-STAT1 signal pathway to promote cancer cell growth, drug resistance, migration, and invasion in breast cancer cells. Although it is known that miR-29b modulates the p38/MAPK pathway, our results reveal that ROS may mediate this pathway. However, further investigations are required to clarify the molecular mechanisms underneath.

Using this model, we identified miR-29b as the top downregulated microRNA in radioresistant cervical cancer cells. Interestingly, miR-29b can regulate PTEN expression. The miR-29b-PTEN axis in radiosensitivity is very specific; blocking endogenous miR-29b in HeLa-R cells abrogates the suppression of PTEN expression and confers radiosensitivity to the cells (Figure 4). Involvement of PTEN in HR-mediated DSB repair has been addressed in several studies;[17,18] however, other studies have completely excluded any role for PTEN in HR.[36,37] It was reported that PTEN defect-associated radioresistance does not fit with the HR-mediated repair, and Fraser et al.[36] also described no effect for PTEN knockdown on HR efficiency or sensitivity to chemotherapy. The discrepancies in the published data could reflect the complexities of regulation of PTEN function in HR. It is possible that miR-29b acts as an important gene responding early to IR and can reverse radioresistance in cervical cancer by directly targeting the PTEN-dependent HR pathway.

PTEN is a natural inhibitor of PI3K by dephosphorylating the 3-phosphate site, and negatively regulates the AKT signaling pathway.[38] But the functions of PTEN-PI3K/AKT signaling in radioresistance, specifically in DNA damage repair, have not been fully elucidated. In this study, we found that IR induction of miR-29b not only suppresses PTEN protein levels but also results in activation of the Akt signaling pathway in cervical cancer (Figure 4A). Our finding provides insights into the mechanism for explaining IR-inducible Akt activation and subsequent cell survival. Most interestingly, our finding demonstrates that the PI3K/Akt inhibitor, which also regulates effectiveness in radiosensitivity of HeLa-R cells, could not be associated with the PTEN-HR-DSB repair pathway (Figures S4 and S5). Paradoxically, it was reported that AKT inhibition recovers the G2/M checkpoint and consequently rescues HR efficiency in PTEN-depleted prostate cancer cells.[38] The discrepancies in the published data concerning the role of AKT in PTEN-HR-DSB repair pathway can be attributed to the fact that PTEN loss is a late event during carcinogenesis, and some additional genomic alterations may occur in a PTEN-independent manner that might mask the role of PTEN in HR. In line with this assumption, we observed that the AKT inactivation showed a partial reverse in PTEN re-expression HeLa-R cells, but no HR-related DSB repair phenotype.

Finally, we confirmed that miR-29b enhanced radiosensitivity in the *in vitro* and *in vivo* radioresistant model of cervical cancer, as demonstrated by assays of tumor growth delay in mice implanted with HeLa-R cervical cancer cells. These findings agree with our *in vitro* findings and demonstrate that miR-29b overexpression significantly

Table 1. R11-SSPEI/miR-29b and Radioresponsiveness of HeLa-R Cells Implanted in Mice Treatment Condition

Treatment[a]	Time to Grow from 5 to 22 mm, Days (mean ± SE)	Absolute Growth Delay (mean ± SE)[b]	Normalized Growth Delay (mean ± SE)[c]	Enhancement Factor[d]
Vehicle	23.5 ± 1.1	–	–	–
R11-SSPEI/Scr	24.4 ± 2.3	0.9 ± 1.3	–	–
R11-SSPEI/miR-29b	25.3 ± 2.5	1.8 ± 1.4	–	–
XRT	29.2 ± 1.5	5.7 ± 1.1	–	–
XRT+R11-SSPEI/Scr	31.1 ± 2.4	7.6 ± 1.3	–	–
XRT+R11-SSPEI/miR-29b	43.6 ± 2.2	20.1 ± 1.1	18.3 ± 0.3	3.2

[a]Five mice per treatment group.
[b]Time (in days) required for tumors to grow from 5 to 22 mm minus time (in days) for tumors to grow from 5 to 22 mm in the untreated control.
[c]Time (in days) required for tumors to grow from 5 to 22 mm in the combination treatment group minus time (in days) for tumors to grow from 5 to 22 mm in the R11-SSPEI/miR-29b-only control.
[d]Normalized growth delay of combination treatment group divided by the absolute growth delay of the radiation-only control.

sensitizes radioresistant cervical cancer cells to radiation. This is also consistent with our hypothesis that miR-29b promotes radiosensitivity by modulating oxidative stress response and by inhibiting PTEN (Figure 6).

In conclusion, we demonstrated that miR-29b increases radiosensitivity in radioresistant cervical cancer cells by regulating the oxidative stress response, and decreases PTEN by inhibiting repair of radiation-induced DSBs. Our *in vivo* experiments support the therapeutic potential of systemic delivery of miR-29b in combination with therapies known to increase oxidative stress, such as radiation.

MATERIALS AND METHODS
Cell Lines and Treatment
The established cervical cancer cell lines Siha, HeLa, Me 180, C-33A, Caski, and normal human cervical epithelial cells (HCvEpC) were obtained from the American Type Culture Collection (Manassas, VA, USA) and cultured in T-medium (GIBCO) supplemented with 5% fetal bovine serum (FBS; GIBCO Invitrogen) at 37°C in a humidified 5% CO_2 incubator.

Synthesis of the R11-SSPEI Nanocarrier
Synthesis of thiolated BPEI (BPEI-SH) and disulfide-crosslinked BPEI (BPEI-SS) was performed as previously described with some modifications.[11] The sample obtained was dissolved in methanol (30 mL) in a bottleneck flask (100 mL) and was purged with nitrogen and kept under a vacuum for 10–20 min. A calculated amount of propylene sulfide (five times the molar excess of BPEI1.2 K) was added using a syringe. This solution was stirred at 60°C for 24 h. The reaction mixture was evaporated to dryness under reduced pressure and was taken up in methanol, followed by precipitation in cold diethyl ether twice. The product's thiol group content was determined using Ellman's method. The BPEI-SH product exhibited a similar kind of proton NMR except for the integral value of protons at d 1. 5e1.2 compared with BPEI1.2 K; 1 H NMR of BPEI-SH (300 MHz, D2O) was d 3. 15e2.55 (m, NCH 2CH 2N, NCH2 CHS) versus 1.5e1.2 (m, CH 3). BPEI-SH
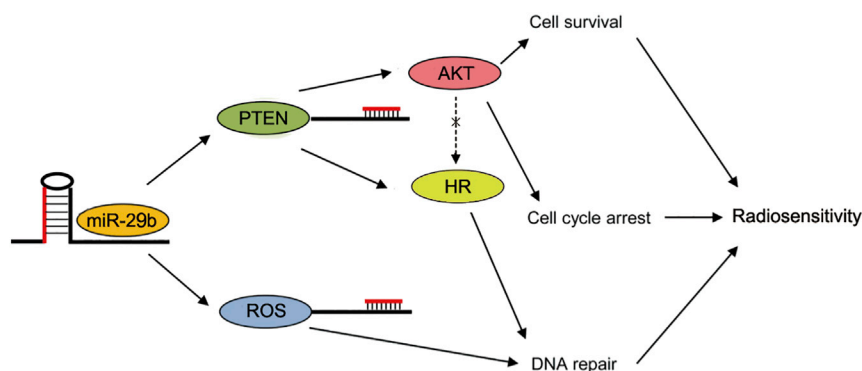
(0.5 g) was dissolved in anhydrous DMSO (50 mL), and the solution was stirred for 48 h at room temperature (RT) for crosslinking via oxidation of the thiol group. The product was purified by dialysis against deionized (D.I.) water (molecular weight cutoff [MWCO] 3500) and extensively lyophilized, and the chemical structure was confirmed by proton NMR. The extent of disulfide crosslinking was determined using Ellman's method. BPEI-SS (12 equiv) and MAL-PEG-NHS were dissolved in 50 mL of anhydrous methanol and DMSO in the proportion of 1:5 (v/v), and this was stirred for 4 h at RT, followed by the addition of R11 peptide (1.2 equiv to MAL-PEG-NHS). The reaction mixture was stirred for another 48 h at RT to afford BPEI-SS-R11. Other experimental and characterization conditions were the same as described above. The R11 peptides (RRRRRRRRRRR) corresponding to protamine were prepared in mass quantities using a peptide synthesizer (APEX 396; AAPP TEC, Louisville, KY, USA) based on standard fluoren-9-ylmethoxycarbonyl (F-moc) chemistry.

Clonogenic Survival Assay
Cervical cancer cells were seeded in triplicate in 60-mm dishes and allowed to stabilize overnight. The next day, the cells were incubated with or without different treatments for 2 h and then irradiated at a dose of 0, 2, 4, or 6 Gy, counted, and seeded in 60-mm dishes. Cells were incubated for 2 weeks. Colonies were fixed and stained for 10 min with 0.5% crystal violet (C3886; Sigma) in methanol. The number of colonies formed in each treatment group was counted. The survival fraction was calculated as: Survival fraction = (plating efficiency of treated cells)/(plating efficiency of control cells), and Plating efficiency = (number of colonies)/(number of cells plated).

Real-Time qPCR
Real-time qPCR was performed to analyze the expression levels of mature microRNAs using TaqMan MicroRNA Reverse Transcription kit (Applied Biosystems) and TaqMan MicroRNA assays kits (Applied Biosystems) according to the manufacturer's protocol. The comparative cycle threshold (Ct) method was used to calculate

Figure 6. The Working Model of Regulation of Radiosensitivity and DNA Damage Repair by miR-29b

in 5% non-fat milk in TBS with Tween 20 (TBS-T). Antibody complexes were detected using the ECL Plus Western Blotting Detection kit (GE Healthcare, UK) and visualized using X-ray film (Laboratory Products Sales). Blots were analyzed using ImageJ software (NIH, Bethesda, MD, USA). Experiments were repeated three times. The relative levels of protein expression were normalized against protein levels of an internal control gene, β-actin, performed in the same run.

the relative abundance of microRNA and mRNAs normalized to U6 and B2M expression, respectively.

Confocal Microscopy Analysis

HeLa cells (1×10^5) that were pre-incubated with the fluorescence CellTracker CM-DiI (Invitrogen) for 20 min were seeded on glass coverslips in 12-well plates and grown for 24 h at 37°C. After the complexation reaction of FAM-labeled miR-29b oligomer with SSPEI or R11-SSPEI for 30 min, this polymer complex was treated into each well and incubated for 1 h. Several washing steps were performed using PBS, and the cells were fixed using 4% paraformaldehyde solution (Wako Pure Chemical, Osaka, Japan) under gentle shaking for 20 min. The fluorescence images were acquired using a confocal laser scanning microscope (LSM 510; Carl Zeiss, Thornwood, NY, USA).

Detection of ROS

In brief, 5×10^5 cells were seeded in six-well plates. The following day, cells were treated with 10 nM R11-SSPEI/29b or R11-SSPEI/Scr for 24 h, and then irradiated to a dose of 0 or 2 Gy. The next day, cells with different treatments were washed with PBS twice and incubated with 20 lM 20, 70-dichlorofluorescein diacetate (DCF-DA; Sigma) for 30 min at 37°C in the dark, and finally were harvested for flow cytometric analyses. The samples were analyzed using FACScan and Cell Quest software (BD Biosciences, Franklin Lakes, NJ, USA) as previously described.[17]

Western Blot Analysis

Western blotting was performed using standard procedures. The cells were washed twice with cold PBS and lysed on ice in radio-immunoprecipitation assay (RIPA) buffer with 1% PMSF (KeyGen, Nanjin, China). The protein lysates were resolved on 10% SDS polyacrylamide gels, transferred to membranes, and blocked in 0.1% Tween 20 and 5% skim milk protein in Tris-buffered saline (TBS). The polyvinylidene fluoride (PVDF) membrane was incubated with primary antibodies: phospho-p38, p38, p-ATF-2, ATF-2, PTEN, AKT, p-AKT (Ser 473), p-AKT (Thr 308), RAD51, β-actin (Santa Cruz, Santa Cruz, CA, USA), and GAPDH (BD PharMingen, San Jose, CA, USA). Secondary horseradish peroxidase (HRP)-conjugated antibodies (Southern Biotech, Birmingham, AL, USA) were incubated

Immunofluorescence Staining

The following day, cells were treated with 10 nM R11-SSPEI/29b or R11-SSPEI/Scr for 24 h, and then irradiated to a dose of 0 or 2 Gy. Cells (0.5×10^5 cells/well) were seeded on glass coverslip in six-well plates. After treatment, cells were washed with PBS, fixed with 4% paraformaldehyde (Sigma-Aldrich), and permeabilized with 0.1% Triton X-100 (Sigma-Aldrich) for 30 min at 37°C. The samples were blocked with 2% BSA (Sigma-Aldrich) for 1 h and incubated with phospho-histone γ-H2AX antibody (Ser139) (Invitrogen) and p53-binding protein 1 (53BP1) antibody (Santa Cruz) overnight at 4°C. Samples were washed and incubated with Alexa Fluor 488-conjugated anti-mouse antibody and Alexa Fluor 594-conjugated anti-rabbit antibody (Invitrogen) for 1 h. Nuclei were counterstained with DAPI (0.2 μg/mL) for 10 min. Then the samples were analyzed under a fluorescence microscope. All samples were examined in three independent experiments.

Cell-Cycle Analysis

Cell cycle was analyzed by flow cytometry. Cells were plated in six wells at a density of 2×10^5 cells. The next day, cells were treated with 10 nM R11-SSPEI/29b or R11-SSPEI/Scr for 24 h and then irradiated to a dose of 2 Gy, and cells with different treatments were incubated at 37°C for 0, 2, 8, and 24 h. Then the treated cells were fixed with cold 70% ethanol for 1 h and stained with 20 μg/mL propidium iodide (PI) (Sigma-Aldrich) containing 1 mg/mL RNase (Sigma-Aldrich) for 1 h. The stained cells were analyzed by an FACSCalibur flow cytometer (Becton Dickinson, San Jose, CA, USA) using the Cell Quest Pro software and WinMDI.

Tumor Radiosensitivity Study

Animal experiments were performed in accordance with a protocol[39] approved by the Institutional Animal Care and Use Committee of Xi'an Jiao Tong University, and mice were euthanized when they met the institutional euthanasia criteria for tumor size and overall health condition. Nude (nu/nu) mice were used for radioresistant cervical cancer xenograft studies. Before tumor cell injection, tumor cell suspensions were prepared from cells grown in monolayers *in vitro*.

HeLa-R tumors were generated by subcutaneous injection of 1×10^6 cells in a volume of 20 µL into the right hind leg of nude mice aged 3–4 months. When tumors grew to 5 mm (range 4.5–5.7 mm) in diameter, mice were assigned to the following groups (10 mice each): Vehicle (no treatment), R11-SSPEI/Scr/miR-29b (five doses of 5 mg/kg each given twice weekly), radiation-only (4 Gy once per day for 5 days, total 20 Gy), or R11-SSPEI/Scr/miR-29b (five 5 mg/kg doses as described above) + radiation. The drugs were given 1 h before radiation. R11-SSPEI/miR-29b is a nanoparticle that contains a synthetic, double-stranded mimic of the tumor suppressor miR-29b.[40] The R11-SSPEI/miR-29b forms a particle with an average diameter of 120 nm and an average zeta-potential of −20 mV. Mice were immobilized in a jig, and tumors were centered in a 3-cm-diameter circular field. All mice were checked twice weekly after irradiation to measure tumor diameter.

For the tumor growth assay, mice were killed when tumors reached 22–25 mm in diameter. Tumor growth delay was defined as the time for tumors to grow from 5 to 25 mm in diameter for treated mice as compared with tumor growth in untreated mice.

Statistical Analysis

Statistical analyses for the data between two groups were determined using Student's t test. Statistics analysis comparisons of more than two groups were evaluated using two-way ANOVA. $p < 0.05$ was considered statistically significant. The statistical software was the SPSS program (version 12.0 for windows; SPSS, Chicago, IL, USA).

SUPPLEMENTAL INFORMATION

Supplemental Information can be found online at https://doi.org/10.1016/j.ymthe.2019.03.020.

AUTHOR CONTRIBUTIONS

H.P. conducted the experiments, X.X. provided foundation, and T.Z. designed the experiments and wrote the paper.

CONFLICTS OF INTEREST

The authors declare no competing interests.

ACKNOWLEDGMENTS

REFERENCES

1. Lee, J., Lin, J.B., Sun, F.J., Chen, Y.J., Chang, C.L., Jan, Y.T., and Wu, M.H. (2017). Safety and efficacy of semiextended field intensity-modulated radiation therapy and concurrent cisplatin in locally advanced cervical cancer patients: An observational study of 10-year experience. Medicine (Baltimore) 96, e6158.

2. Nakamura, K., Masuyama, H., Ida, N., Haruma, T., Kusumoto, T., Seki, N., and Hiramatsu, Y. (2017). Radical Hysterectomy Plus Concurrent Chemoradiation/Radiation Therapy Is Negatively Associated With Return to Work in Patients With Cervical Cancer. Int. J. Gynecol. Cancer 27, 117–122.

3. Osborne, E.M., Klopp, A.H., Jhingran, A., Meyer, L.A., and Eifel, P.J. (2017). Impact of treatment year on survival and adverse effects in patients with cervical cancer and paraortic lymph node metastases treated with definitive extended-field radiation therapy. Pract. Radiat. Oncol. 7, e165–e173.

4. Tavazoie, S.F., Alarcón, C., Oskarsson, T., Padua, D., Wang, Q., Bos, P.D., Gerald, W.L., and Massagué, J. (2008). Endogenous human microRNAs that suppress breast cancer metastasis. Nature 451, 147–152.

5. Svoronos, A.A., Engelman, D.M., and Slack, F.J. (2016). OncomiR or Tumor Suppressor? The Duplicity of MicroRNAs in Cancer. Cancer Res. 76, 3666–3670.

6. Rossbach, M. (2012). MicroRNAs in cancer therapy. Expert Opin. Ther. Targets 16, 743–745.

7. Balzeau, J., Menezes, M.R., Cao, S., and Hagan, J.P. (2017). The LIN28/let-7 Pathway in Cancer. Front. Genet. 8, 31.

8. Abba, M.L., Patil, N., Leupold, J.H., Moniuszko, M., Utikal, J., Niklinski, J., and Allgayer, H. (2017). MicroRNAs as novel targets and tools in cancer therapy. Cancer Lett. 387, 84–94.

9. Ping, W., Gao, Y., Fan, X., Li, W., Deng, Y., and Fu, X. (2018). MiR-181a contributes gefitinib resistance in non-small cell lung cancer cells by targeting GAS7. Biochem. Biophys. Res. Commun. 495, 2482–2489.

10. Du, X.Y., Hu, Y.Y., Xie, C., Deng, C.Y., Liu, C.Y., Luo, Z.G., Niu, Y.M., and Shen, M. (2017). Significant association between Let-7-KRAS rs712 G > T polymorphism and cancer risk in the Chinese population: a meta-analysis. Oncotarget 8, 13863–13871.

11. Shinden, Y., Iguchi, T., Akiyoshi, S., Ueo, H., Ueda, M., Hirata, H., Sakimura, S., Uchi, R., Takano, Y., Eguchi, H., et al. (2015). miR-29b is an indicator of prognosis in breast cancer patients. Mol. Clin. Oncol. 3, 919–923.

12. Inoue, A., Mizushima, T., Wu, X., Okuzaki, D., Kambara, N., Ishikawa, S., Wang, J., Qian, Y., Hirose, H., Yokoyama, Y., et al. (2018). A miR-29b Byproduct Sequence Exhibits Potent Tumor-Suppressive Activities via Inhibition of NF-κB Signaling in KRAS-Mutant Colon Cancer Cells. Mol. Cancer Ther. 17, 977–987.

13. Hou, M., Zuo, X., Li, C., Zhang, Y., and Teng, Y. (2017). Mir-29b Regulates Oxidative Stress by Targeting SIRT1 in Ovarian Cancer Cells. Cell. Physiol. Biochem. 43, 1767–1776.

14. Yan, B., Guo, Q., Fu, F.J., Wang, Z., Yin, Z., Wei, Y.B., and Yang, J.R. (2015). The role of miR-29b in cancer: regulation, function, and signaling. OncoTargets Ther. 8, 539–548.

15. Jia, L.F., Huang, Y.P., Zheng, Y.F., Lyu, M.Y., Wei, S.B., Meng, Z., and Gan, Y.H. (2014). miR-29b suppresses proliferation, migration, and invasion of tongue squamous cell carcinoma through PTEN-AKT signaling pathway by targeting Sp1. Oral Oncol. 50, 1062–1071.

16. Dai, F., Zhang, Y., Zhu, X., Shan, N., and Chen, Y. (2012). Anticancer role of MUC1 aptamer-miR-29b chimera in epithelial ovarian carcinoma cells through regulation of PTEN methylation. Target. Oncol. 7, 217–225.

17. Gupta, A., Yang, Q., Pandita, R.K., Hunt, C.R., Xiang, T., Misri, S., Zeng, S., Pagan, J., Jeffery, J., Puc, J., et al. (2009). Cell cycle checkpoint defects contribute to genomic instability in PTEN deficient cells independent of DNA DSB repair. Cell Cycle 8, 2198–2210.

18. Saal, L.H., Gruvberger-Saal, S.K., Persson, C., Lövgren, K., Jumppanen, M., Staaf, J., Jönsson, G., Pires, M.M., Maurer, M., Holm, K., et al. (2008). Recurrent gross mutations of the PTEN tumor suppressor gene in breast cancers with deficient DSB repair. Nat. Genet. 40, 102–107.

19. Shin, J., Shim, H.G., Hwang, T., Kim, H., Kang, S.H., Dho, Y.S., Park, S.H., Kim, S.J., and Park, C.K. (2017). Restoration of miR-29b exerts anti-cancer effects on glioblastoma. Cancer Cell Int. 17, 104.

20. Liu, Q., Tao, B., Liu, G., Chen, G., Zhu, Q., Yu, Y., Yu, Y., and Xiong, H. (2016). Thromboxane A2 Receptor Inhibition Suppresses Multiple Myeloma Cell Proliferation by Inducing p38/c-Jun N-terminal Kinase (JNK) Mitogen-activated Protein Kinase (MAPK)-mediated G2/M Progression Delay and Cell Apoptosis. J. Biol. Chem. 291, 4779–4792.

21. Saldeen, J., Lee, J.C., and Welsh, N. (2001). Role of p38 mitogen-activated protein kinase (p38 MAPK) in cytokine-induced rat islet cell apoptosis. Biochem. Pharmacol. 61, 1561–1569.

22. Qi, Y., Huang, Y., Pang, L., Gu, W., Wang, N., Hu, J., Cui, X., Zhang, J., Zhao, J., Liu, C., et al. (2017). Prognostic value of the MicroRNA-29 family in multiple human cancers: A meta-analysis and systematic review. Clin. Exp. Pharmacol. Physiol. 44, 441–454.

23. Li, Y., Cai, B., Shen, L., Dong, Y., Lu, Q., Sun, S., Liu, S., Ma, S., Ma, P.X., and Chen, J. (2017). MiRNA-29b suppresses tumor growth through simultaneously inhibiting angiogenesis and tumorigenesis by targeting Akt3. Cancer Lett. *397*, 111–119.

24. Zhu, K., Liu, L., Zhang, J., Wang, Y., Liang, H., Fan, G., Jiang, Z., Zhang, C.Y., Chen, X., and Zhou, G. (2016). MiR-29b suppresses the proliferation and migration of osteosarcoma cells by targeting CDK6. Protein Cell *7*, 434–444.

25. Li, Y., Zhang, Z., Xiao, Z., Lin, Y., Luo, T., Zhou, Q., and Zhang, X. (2017). Chemotherapy-mediated miR-29b expression inhibits the invasion and angiogenesis of cervical cancer. Oncotarget *8*, 14655–14665.

26. Liu, H., and Cheng, X.H. (2018). MiR-29b reverses oxaliplatin-resistance in colorectal cancer by targeting SIRT1. Oncotarget *9*, 12304–12315.

27. Sugio, A., Iwasaki, M., Habata, S., Mariya, T., Suzuki, M., Osogami, H., Tamate, M., Tanaka, R., and Saito, T. (2014). BAG3 upregulates Mcl-1 through downregulation of miR-29b to induce anticancer drug resistance in ovarian cancer. Gynecol. Oncol. *134*, 615–623.

28. Basati, G., Razavi, A.E., Pakzad, I., and Malayeri, F.A. (2016). Circulating levels of the miRNAs, miR-194, and miR-29b, as clinically useful biomarkers for colorectal cancer. Tumour Biol. *37*, 1781–1788.

29. Bahador, R., Taheriazam, A., Mirghasemi, A., Torkaman, A., Shakeri, M., Yahaghi, E., and Goudarzi, P.K. (2016). Retraction. Tumour Biol. *37*, 16407.

30. Zhang, T., Xue, X., He, D., and Hsieh, J.T. (2015). A prostate cancer-targeted polyarginine-disulfide linked PEI nanocarrier for delivery of microRNA. Cancer Lett. *365*, 156–165.

31. Chung, H.J., Choi, Y.E., Kim, E.S., Han, Y.H., Park, M.J., and Bae, I.H. (2015). miR-29b attenuates tumorigenicity and stemness maintenance in human glioblastoma multiforme by directly targeting BCL2L2. Oncotarget *6*, 18429–18444.

32. Xu, Z., Zhang, L., Fei, X., Yi, X., Li, W., and Wang, Q. (2014). The miR-29b-Sirt1 axis regulates self-renewal of mouse embryonic stem cells in response to reactive oxygen species. Cell. Signal. *26*, 1500–1505.

33. Li, C., and Jackson, R.M. (2002). Reactive species mechanisms of cellular hypoxia-reoxygenation injury. Am. J. Physiol. Cell Physiol. *282*, C227–C241.

34. Zhao, W., Lu, M., and Zhang, Q. (2015). Chloride intracellular channel 1 regulates migration and invasion in gastric cancer by triggering the ROS-mediated p38 MAPK signaling pathway. Mol. Med. Rep. *12*, 8041–8047.

35. Liu, Y., Zhang, J., Sun, X., Su, Q., and You, C. (2017). Down-regulation of miR-29b in carcinoma associated fibroblasts promotes cell growth and metastasis of breast cancer. Oncotarget *8*, 39559–39570.

36. Fraser, M., Zhao, H., Luoto, K.R., Lundin, C., Coackley, C., Chan, N., Joshua, A.M., Bismar, T.A., Evans, A., Helleday, T., Bristow, R.G., et al. (2012). PTEN deletion in prostate cancer cells does not associate with loss of RAD51 function: implications for radiotherapy and chemotherapy. Clin. Cancer Res. *18*, 1015–1027.

37. Pappas, G., Zumstein, L.A., Munshi, A., Hobbs, M., and Meyn, R.E. (2007). Adenoviral-mediated PTEN expression radiosensitizes non-small cell lung cancer cells by suppressing DNA repair capacity. Cancer Gene Ther. *14*, 543–549.

38. Mansour, W.Y., Tennstedt, P., Volquardsen, J., Oing, C., Kluth, M., Hube-Magg, C., Borgmann, K., Simon, R., Petersen, C., Dikomey, E., and Rothkamm, K. (2018). Loss of PTEN-assisted G2/M checkpoint impedes homologous recombination repair and enhances radio-curability and PARP inhibitor treatment response in prostate cancer. Sci. Rep. *8*, 3947.

39. Zhang, T., Zhang, L., Zhang, T., Fan, J., Wu, K., Guan, Z., Wang, X., Li, L., Hsieh, J.T., He, D., and Guo, P. (2014). Metformin sensitizes prostate cancer cells to radiation through EGFR/p-DNA-PKCS in vitro and in vivo. Radiat. Res. *181*, 641–649.

40. Cortez, M.A., Valdecanas, D., Zhang, X., Zhan, Y., Bhardwaj, V., Calin, G.A., Komaki, R., Giri, D.K., Quini, C.C., Wolfe, T., et al. (2014). Therapeutic delivery of miR-200c enhances radiosensitivity in lung cancer. Mol. Ther. *22*, 1494–1503.